



ISTITUTO NAZIONALE DI RICERCA METROLOGICA Repository Istituzionale

A New Industry-Oriented Technique for the Wideband Characterization of Voltage Transformers

Original

A New Industry-Oriented Technique for the Wideband Characterization of Voltage Transformers / Crotti, G.; Giordano, D.; D'Avanzo, G.; Letizia, P. S.; Luiso, M.. - In: MEASUREMENT. - ISSN 0263-2241. - 182:(2021), p. 109674. [10.1016/j.measurement.2021.109674]

Availability:

This version is available at: 11696/74210 since: 2022-04-12T13:27:54Z

Publisher:

ELSEVIER SCI LTD

Published

DOI:10.1016/j.measurement.2021.109674

Terms of use:

This article is made available under terms and conditions as specified in the corresponding bibliographic description in the repository

Publisher copyright

(Article begins on next page)



A New Industry-Oriented Technique for the Wideband Characterization of Voltage Transformers

G. Crotti^a, D. Giordano^a, G. D'Avanzo^b, P.S. Letizia^{a,c,*}, M. Luiso^b

^a Istituto Nazionale di Ricerca Metrologica, Torino, Italy

^b Università degli studi della Campania "Luigi Vanvitelli", Aversa (CE), Italy

^c Politecnico di Torino, Torino, Italy

ARTICLE INFO

Keywords:

Voltage transformer
Power system measurements
SINDICOMP-LV
Harmonics
Frequency response
Non-linearity

ABSTRACT

The constant increase of switching power converters in distribution and transmission grids pushes the need for harmonic measurements. Recent literature has shown that inductive Voltage and Current Instrument Transformers (VTs and CTs) can be used for harmonic measurements, but their accurate frequency characterization involves the use of quite costly instrumentation. In this context, this paper proposes an industry oriented technique for frequency characterization of medium voltage inductive VTs, involving instrumentation that, typically, is present in accredited laboratories or at VT manufacturers premises. In fact, it requires the generation of only sine waves and the measurement of: i) ratio and phase errors in sinusoidal rated conditions, the same prescribed by the international standards, and ii) ratio and phase errors with sine waves at 7 V from power frequency up to the first resonance frequency. The proposed technique, named SINDICOMP-LV, has been applied to medium voltage VTs and validated by the INRIM reference system for frequency characterization of VTs. Accuracy improvement with respect to the use of a conventional low voltage frequency sweep is up to one order of magnitude for the ratio error and up to 5 mrad for the phase over the considered frequency ranges, depending on the frequency value

1. Introduction

High-frequency power converters, electronic non-linear loads, decentralized renewable energy sources are among the underlying causes of the significant increase of power grid harmonic pollution [1,2].

As a result, harmonic level assessment is a matter of growing importance for several power grid applications such as metering, monitoring, protection, and control [3]. In medium voltage (MV) and high voltage (HV) grids, the quantification of the harmonic levels can strongly depend on the performance and accuracy of the measurement chain, which must always include sensors to reduce voltage and current to amplitude levels compliant with the low voltage (LV) input of the harmonic measuring instrument. For economic and practical reasons, inductive instrument transformers (ITs), installed in HV and MV grids for metering and protection applications, are frequently used also for harmonics and, more generally, for power quality (PQ) measurements [4,5].

Recent literature [5–13] has shown that the frequency performance of ITs is affected both by their intrinsic non-linearity and by stray capacitance, so that non-negligible ratio and phase errors (up to some percent and tens of milliradians) can be introduced both at low and high frequency harmonics. Consequently, IT ratio and phase errors measured by performing a frequency sweep at low voltage under sinusoidal supply can significantly differ from those measured by using waveforms more representative of realistic operating conditions [13,14]. To this end, distorted waveforms, composed of a fundamental tone at rated voltage amplitude plus one or N superimposed harmonic tones with reduced amplitudes can be used. However, these tests require quite complex and expensive setups for both the generation and reference measurement chain sections.

Another important aspect to point out is that, at now, no international standard, in particular the IEC 61869 family [15–17] focused on ITs, gives indications on how to test the IT performances at frequencies different from the fundamental one. On this subject, the EMPIR19NRM05 IT4PQ project [18,19] recently started, aiming to fill the present knowledge gaps and support the development of

* Corresponding author.

E-mail addresses: g.crotti@inrim.it (G. Crotti), d.giordano@inrim.it (D. Giordano), giovanni.davanzo@unicampania.it (G. D'Avanzo), p.letizia@inrim.it (P.S. Letizia), mario.luiso@unicampania.it (M. Luiso).

<https://doi.org/10.1016/j.measurement.2021.109674>

Received 29 January 2021; Received in revised form 16 April 2021; Accepted 27 May 2021

Available online 6 June 2021

0263-2241/© 2021 The Authors.

Published by Elsevier Ltd.

This is an open access article under the CC BY-NC-ND license

(<http://creativecommons.org/licenses/by-nc-nd/4.0/>).

Nomenclature

List of Symbols

Symbol Description

f	Frequency.
f_1	Fundamental frequency
hf_1	h -th harmonic frequency
f_R	First resonance frequency of a VT
f_{start}	First frequency of the interval used for fitting procedure
f_{stop}	Last frequency of the interval used for fitting procedure
m	Factor used to select f_{start}
a	Parameter used in the fitting procedure
b	Parameter used in the fitting procedure
$\bar{V}_p(hf_1)$	Phasor of the primary voltage at hf_1
$V_p(hf_1)$	Magnitude of the phasor of the primary voltage at hf_1
$\angle \bar{V}_p(hf_1)$	Phase angle of the phasor of the primary voltage at hf_1
$\bar{V}_p^{\text{sin}}(hf_1)$	Phasor of the VT primary voltage at hf_1 under sine wave condition.
$\bar{V}_p^{\text{d}}(hf_1)$	Phasor of the VT primary voltage at hf_1 under distorted waveform conditions
$\bar{V}_s(hf_1)$	Phasor of the secondary voltage at hf_1
$V_s(hf_1)$	Magnitude of the phasor of the secondary voltage at hf_1
$\angle \bar{V}_s(hf_1)$	Phase angle of the phasor of the secondary voltage at hf_1
$\bar{V}_s^{\text{sin}}(hf_1)$	Phasor of the VT secondary voltage at hf_1 under sine wave conditions
$\bar{V}_s^{\text{d}}(hf_1)$	Phasor of the VT secondary voltage at hf_1 under distorted waveform conditions
$\dot{k}(f)$	Complex ratio of the VT at f
k_r	Rated ratio of the VT

$\Delta\varphi(f)$	Phase Error at f
$\varepsilon(f)$	Ratio Error at f
$\Delta\varphi_{\text{MV}}(f)$	Phase Error, at f , in a MV reference test
$\varepsilon_{\text{MV}}(f)$	Ratio Error, at f , in a MV reference test
$\Delta\varphi_{\text{FH1}}(f)$	Phase Error, at f , in a FH1 test
$\varepsilon_{\text{FH1}}(f)$	Ratio Error, at f , in a FH1 test
$\varepsilon_{\text{FH1,rb}}(f)$	Ratio Error with rated burden, at f , in a FH1 test
$\Delta\varphi_{\text{LV}}(f)$	Phase Error, at f , in a LV test
$\varepsilon_{\text{LV}}(f)$	Ratio Error, at f , in a LV test
$\Delta\varphi_{\text{FIT}}(f)$	Phase Error, at f , obtained through the fit procedure
$\varepsilon_{\text{FIT}}(f)$	Ratio Error, at f , obtained through the fit procedure
$\Delta\varphi_{\text{S-LV}}(f)$	Phase Error, at f , obtained by applying S-LV
$\varepsilon_{\text{S-LV}}(f)$	Ratio Error, at f , obtained by applying S-LV
$\delta_{\text{LV}}(f)$	Ratio error deviations, at f , between the errors obtained at LV and by the FH1 test
$\delta_{\text{LV}}(f)$	Phase error deviations, at f , between the errors obtained at LV and by the MV FH1 test
$\delta_{\text{S-LV}}(f)$	Ratio error deviations, at f , between the errors obtained with S-LV and by the FH1 test
$\delta_{\text{S-LV}}(f)$	Phase error deviations, at f , between the errors obtained with S-LV and by the FH1 test
$\delta_{\text{LV,rb}}(f)$	Ratio error deviations with rated burden, at f , between the errors obtained at LV and by the FH1 test
$\delta_{\text{LV,rb}}(f)$	Phase error deviations with rated burden, at f , between the errors obtained at LV and by the FH1 test
$\delta_{\text{S-LV,rb}}(f)$	Ratio error deviations with rated burden, at f , between the errors obtained with S-LV and by the FH1 test
$\delta_{\text{S-LV,rb}}(f)$	Phase error deviations with rated burden, at f , between the errors obtained with S-LV and by the FH1 test

standardized procedures, focused on the characterization of the ITs used for PQ measurements. In this context, this paper aims at finding a tradeoff between complex and expensive test procedures, such as those proposed in [5–13] and simpler, but less accurate, low voltage ones.

Some of the authors in [20,21], already presented two different techniques to obtain an approximated frequency response for the voltage instrument transformer (VT) ratio error, both based on two steps involving only sine waves: i) characterization at rated amplitude and frequency and application of SINDICOMP (SINusoidal characterization for DIstortion COMPensation) for the compensation of low frequency non-linearity (up to some hundreds of hertz); ii) execution of a LV frequency sweep and use of these data to approximate the VT frequency response. Differently from [5–13], these techniques [20,21] can be easily implemented by making use of generation and measurement setups already available in IT calibration laboratories, even if the reconstructed frequency responses are not so accurate as those obtained in [5–13].

Therefore, this paper starting from [21] presents an enhanced technique that allows building an approximated VT complex frequency response, up to the first resonance frequency, by using exclusively sine waves and thus involving generation and measurement setups already available in ITs calibration laboratories.

The proposed approach builds on the observation that the frequency region from 50 Hz up to the first resonance frequency can be split in two regions:

- from 50 Hz up to f_{start} (in Section 3 more details will be given about this frequency value) where the VT behavior is strongly non-linear,
- from f_{start} up the first resonance frequency where the VT behavior can be considered linear.

Section 2 better explains these phenomena.

Starting from this consideration, the approach proposed in the paper is based on these three simple steps:

- measurement of VT ratio and phase errors at rated voltage and rated frequency;
- measurement of the VT ratio and phase frequency behavior at low voltage up to the first resonance frequency;
- use of a suitable algorithm (as detailed in Section 3) combining the two sets of data to obtain an approximated VT complex frequency response.

In the following, we refer to the proposed procedure as SINDICOMP-LV (SINDICOMP plus Low Voltage characterization for Wideband harmonic measurements), or simply S-LV, as it builds on SINDICOMP procedure, but integrates and extends it to a wider frequency range by using LV sine waves. With respect to the previous techniques, S-LV gives a more accurate reconstruction of the magnitude of the VT frequency response and it works well also in the reconstruction of the VT phase behavior. Moreover, the procedure is proved to work accurately even when the LV frequency sweep is performed at low voltage levels, i.e. 7 V, which further reduce the requirements for the instrumentations. The S-LV is applied to three commercial VTs for MV applications, with different rated primary voltage and the results are validated by comparison with measurements carried out with INRIM reference system. In addition, to verify the robustness of S-LV, a sensitivity analysis considering different parameters and including the burden of the VT, is presented.

The paper is organized as follows. Section 2 gives some background considerations about VT non-linearity. Section 3 discusses SINDICOMP-LV and its application to VT magnitude and phase frequency response

approximation. Section 4 shows the measurement procedure and setup. Section 5 presents the application of S-LV to three different commercial VTs, whereas in Section 6 the S-LV sensitivity analysis is provided. Section 7 gives a general discussion on the results. Finally, Section 8 draws the conclusions.

2. Background considerations about VT non-linearity

One of the limit of using conventional inductive VTs in power grid applications is the non-linearity introduced by their iron-core. Two main effects of such a non-linearity are briefly discussed in the following. The first one can be observed in Fig. 1 by comparing the frequency behavior of the VT ratio error, under increasing applied LV amplitudes (tens to some hundreds of volt), with the error obtained by applying a fundamental tone at rated voltage and frequency, with a superimposed harmonic frequency sweep (FH1, Fig. 1). The differences can be explained considering that, when the VT is tested at low voltage, the magnetization of the iron core is low compared with the rated operating point and such are the iron losses, which depend on the supply voltage and frequency. Iron core effects can be introduced in a common circuital model of a transformer by selecting, for each supply frequency, a different value of the magnetization inductance and of the resistance that emulates the actual losses.

With the increase of the frequency, the effect of the stray capacitances among turns and between windings and ground starts to predominate on the non-linear effects, as shown in Fig. 1 where, beyond a certain frequency, the behavior of the ratio error can be considered independent from the supply voltage. The second effect is visible up to the first harmonics (some hundreds of hertz) when the rated primary voltage is applied. We can note that the ratio error obtained by applying the rated voltage at f_1 with a superimposed third harmonic, varying its phase angle with respect to the fundamental one, shows a nearly sinusoidal behavior (see Fig. 2). This effect is due to the combination of the harmonic applied to the input of the VT and the third harmonic generated by the fundamental tone, because of the non-linearity of the VT $B-H$ curve. By SINDICOMP method [9] such a non-linearity can be quite satisfactorily compensated at the rated supply voltage as shown in Fig. 2.

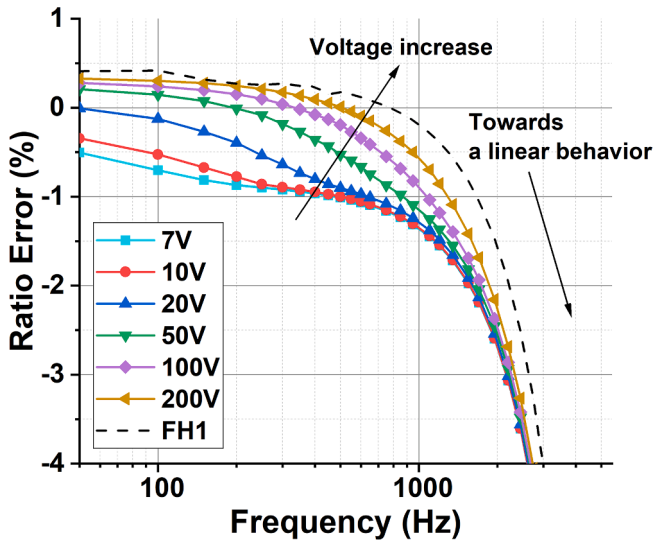


Fig. 1. Ratio errors frequency behavior obtained with various low voltage amplitudes and FH1 response (reference frequency response measured at rated voltage plus harmonic).

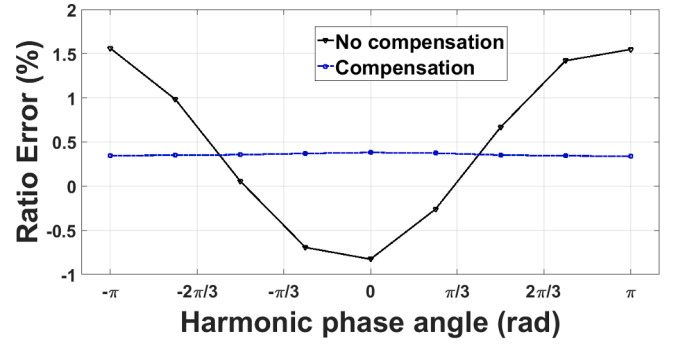


Fig. 2. Ratio error associated with the applied third harmonic versus its phase angle displacement with respect to the fundamental tone without and with the compensation method SINDICOMP.

3. SINDICOMP-LV: SINDICOMP with Low Voltage sinusoidal frequency sweep

3.1. Scope of the technique

The scope of the frequency characterization of a VT is to determine its actual complex transformation ratio $\hat{k}(f)$, expressed by

$$\hat{k}(f) = \frac{\bar{V}_p(f)}{\bar{V}_s(f)} \quad (1)$$

where $\bar{V}_p(f)$ and $\bar{V}_s(f)$ are respectively the phasor representation of the primary and secondary voltage at the frequency f . Being k_r the rated VT transformation ratio, the VT ratio error $\varepsilon(f)$ and phase error $\Delta\varphi(f)$ are obtained according to [17]:

$$\varepsilon(f) = \frac{k_r \cdot V_s(f) - V_p(f)}{V_p(f)} = \frac{k_r}{k(f)} - 1 \quad (2)$$

$$\Delta\varphi(f) = \angle V_s(f) - \angle V_p(f) = -\angle \hat{k}(f) \quad (3)$$

where $V_p(f)$ and $V_s(f)$ are the magnitudes of the $\bar{V}_p(f)$ and $\bar{V}_s(f)$ phasors and $\Delta\varphi(f)$ is the phase displacement. As discussed in Section 2, the measured VT magnitude $k(f)$ and phase $\Delta\varphi(f)$ or the VT ratio $\varepsilon(f)$ and phase $\Delta\varphi(f)$ errors, are dependent on the applied primary voltage, especially at low frequencies (up to some hundreds of hertz) due to the non-linear behaviour of the VT magnetic core. Determination of their values at the rated voltage under distorted waveform requires the use of expensive generation and measurement capabilities that, typically, are not present in accredited laboratories for IT calibration or internal laboratories of IT manufacturers [5–13].

Therefore, a specific procedure is here presented, S-LV that, starting from the VT harmonic ratio and phase errors measured with a LV AC frequency sweep ($\varepsilon_{LV}(f)$, $\Delta\varphi_{LV}(f)$), aims at the estimation of a VT “improved” frequency response, with ratio and phase errors ($\varepsilon_{S-LV}(f)$, $\Delta\varphi_{S-LV}(f)$), significantly closer to those occurring under distorted MV waveforms ($\varepsilon_{MV}(f)$, $\Delta\varphi_{MV}(f)$) so that:

$$|\varepsilon_{S-LV}(f) - \varepsilon_{MV}(f)| < |\varepsilon_{LV}(f) - \varepsilon_{MV}(f)| \quad (4)$$

$$|\Delta\varphi_{S-LV}(f) - \Delta\varphi_{MV}(f)| < |\Delta\varphi_{LV}(f) - \Delta\varphi_{MV}(f)| \quad (5)$$

It is worth to underline that this target is obtained by using instrumentation already present in industry laboratories.

3.2. SINDICOMP

The preliminary step of S-LV is the application of the SINDICOMP procedure [9]. Therefore, here a summary of this procedure is given.

Sinusoidal voltages, with amplitudes from 80% to 120% of the rated VT voltage and frequency f_1 , are applied to the VT. The magnitude and

phase of the phasors $\bar{V}_p^{\sin}(f_1)$, $\bar{V}_s^{\sin}(f_1)$ and the errors $\varepsilon(f_1)$, $\Delta\varphi(f_1)$ are measured and stored in look-up tables.

Then, in the practical use of the VT at MV, likely to involve distorted waveforms, the primary phasors can be reconstructed from the secondary phasors:

$$\bar{V}_p^d(hf_1) = k_r \cdot \left(\bar{V}_s^d(hf_1) - \bar{V}_s^{\sin}(hf_1) \right) \quad (6)$$

where $\bar{V}_s^d(hf_1)$ is the secondary voltage phasor measured at the harmonic order h under distorted MV conditions and the phase angles of the secondary harmonic phasors are defined as:

$$\angle \bar{V}_s^d(hf_1) = \angle \bar{V}_s^d(hf_1) \Big|_{FFT} - \angle \bar{V}_s^{\sin}(hf_1) \quad (7)$$

where $\angle \bar{V}_s^d(hf_1) \Big|_{FFT}$ is the h harmonic phase angle provided by the FFT algorithm. With this preliminary step, the VT behavior, both in terms of ratio as well as phase errors is measured at rated frequency f_1 , in addition, the non-linearity effect (see Fig. 2), observable at the frequencies up to some hundreds of hertz, is strongly reduced.

It must be highlighted that the tests with amplitudes from 80% to 120% of the rated VT voltage and at rated frequency f_1 are prescribed by the relevant standards [15–17]. Thus, this preliminary S-LV step does not involve any additional test other than those already indicated for a VT calibration, with the exception of an analysis in the frequency domain of the secondary voltages, whose time waveforms, if not already available, have to be synchronously recorded.

3.3. Ratio error approximation

The second step of the S-LV procedure involves the measurement of the low voltage frequency response of the VT in terms of $\varepsilon_{LV}(f)$ and $\Delta\varphi_{LV}(f)$ by performing a sinusoidal frequency sweep (LV test), for example at 7 V.

From Fig. 1 we can see that $\varepsilon_{LV}(f)$, especially for very low voltage levels, is not able to accurately describe the VT magnitude behaviour under rated conditions, since it is quite far from the “true value” $\varepsilon_{MV}(f)$, which is estimated by carrying out a FH1 MV test, as described in the previous section ($\varepsilon_{MV}(f) = \varepsilon_{FH1}(f)$). Same consideration can be made for $\Delta\varphi_{LV}$. However, as can be noted in Fig. 1, with the increase of the frequency, the shapes of ε_{LV} and ε_{FH1} curves become quite similar.

So, considering the $\varepsilon_{LV}(f)$ frequency behavior, the following fit function is here used:

$$\varepsilon_{FIT}(f) = \frac{\sqrt{(2\pi f a)^2 + b^2}}{\sqrt{\left(1 - (f/f_R)^2\right)^2 + (f/2\pi f_R^2 \cdot b/a)^2}} \quad (8)$$

where f_R is the first resonance frequency, whose value is obtained from the measured $\varepsilon_{LV}(f)$, and a and b are fit parameters. It must be underlined that the simplified model (8) is not the VT real one and the parameters a and b are determined by fitting to the experimental frequency response data, implementing a grey box approach.

To provide good results, the fitting procedure must be carried out in a frequency range $[f_{start}, f_{stop}]$ where the linear effects are predominant on the non-linear behaviour. As regards f_{stop} , it must be considered that the use of fitting function (8) next to and beyond the resonance frequency can lead to unsatisfactory results. Following this consideration, we fixed f_{stop} as:

$$f_{stop} = f_R - 1 \text{ kHz} \quad (9)$$

limiting the range to 1 kHz before reaching f_R . The value of f_R , can be properly identified through a LV test at 7 V [22].

Then, in order to delimit a frequency range where the VT behaviour

is predominantly linear, so excluding the lower frequencies, a possible choice for f_{start} could stem from halving the interval $[f_1, f_R]$, that is choosing f_{start} as:

$$f_{start} \approx (f_R - f_1)/m, \quad m = 2 \quad (10)$$

However, experimental results on different VTs, as also shown in section VI, suggest that a good choice for f_{start} is:

$$f_{start} \approx (f_R - f_1)/m, \quad m = 2.5 \quad (11)$$

This corresponds to a little enlargement of the frequency range used for the fitting procedure. In section 6 it will be also demonstrated that dividing $(f_R - f_1)$ by a factor m included in the range 2 to 3 does not significantly affect the S-LV accuracy. This consideration, indeed, helps the user: in fact, a VT is typically characterized at harmonic frequency points $f = h \cdot f_1$, where h is the harmonic order. In this case the equation (10) could lead to a f_{start} value not exactly corresponding to a harmonic frequency. In this respect, rounding f_{start} to the nearest harmonic frequency does not significantly affect the accuracy of SINDICOMP for this reason (10) and (11) are approximate equalities.

After the definition of the frequency interval $[f_{start}, f_{stop}]$, the function $\varepsilon_{FIT}(f)$ is identified by non-linear least squares analysis using the experimental $\varepsilon_{LV}(f)$ data in the considered interval; the outputs of the fitting procedure are the numerical values of a and b parameters.

The fit function has then to be modified to take into account the actual VT response at the lowest frequency, where the VT non-linearities are predominant. This is done by adding an offset correction $\varepsilon_{OFS,a}$, ideal computed as:

$$\varepsilon_{OFS,a} = \varepsilon_{MV}(f_1) - \varepsilon_{FIT}(f_1) \quad (12)$$

where $\varepsilon_{MV}(f_1)$ is set equal to the ratio error value measured during the standard calibration at rated frequency, carried out at prescribed voltage in the preliminary step [17] (see section 3.2).

The final VT approximated ratio error $\varepsilon_{S-LV}(f)$ is then assumed equal to $\varepsilon_{FIT}(f) + \varepsilon_{OFS,a}$ up to f_{start} . From this frequency on, the VT is assumed linear and its ratio error frequency response $\varepsilon_{S-LV}(f)$ is considered equal to the response $\varepsilon_{LV}(f)$ shifted of the quantity $\varepsilon_{OFS,b}$, obtained as:

$$\varepsilon_{OFS,b} = \varepsilon_{FIT}(f_{start}) + \varepsilon_{OFS,a} - \varepsilon_{LV}(f_{start}) \quad (13)$$

Summarizing, the approximated ratio error $\varepsilon_{S-LV}(f)$ is then obtained as:

$$\varepsilon_{S-LV}(f) = \begin{cases} \varepsilon_{FIT}(f) + \varepsilon_{OFS,a} & f_1 \leq f < f_{start} \\ \varepsilon_{LV}(f) + \varepsilon_{OFS,b} & f_{start} \leq f < f_{stop} \end{cases} \quad (14)$$

The graphical representation of the S-LV steps for the identification of the VT ratio error is shown in Fig. 3, where the involved ratio error curves versus frequency are shown. The error frequency response

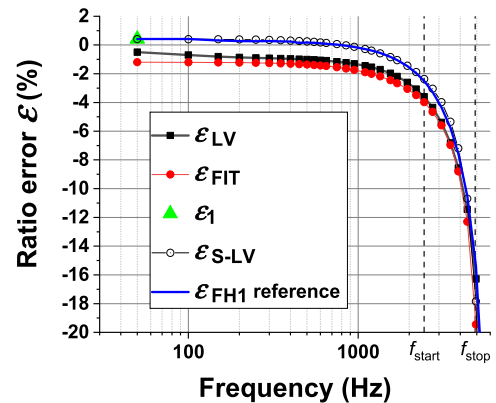


Fig. 3. Graphical description of the fitting procedure for the identification of the VT ratio error frequency response.

obtained under FH1 MV frequency sweep is also shown for comparison.

3.4. Phase error approximation

For the phase error approximation the same approach is adopted: $\Delta\varphi_{LV}(f)$ and f_R quantities are those measured in the LV test and the parameters f_{start} , f_{stop} , a and b are the ones identified in the ratio error fit procedure. The function used for phase error approximation is set to:

$$\Delta\varphi_{FIT}(f) = \arctan\left(2\pi f \cdot \frac{a}{b}\right) - \arctan\left(\frac{\frac{f}{2\pi f_R^2} \cdot \frac{b}{a}}{\left(1 - \left(\frac{f}{f_R}\right)^2\right)^2}\right) + 2\pi f \cdot \frac{a}{b} \quad (15)$$

Same as for the ratio error, $\Delta\varphi_{FIT}(f)$ is shifted for offset $\Delta\varphi_{OFS,a}$ and computed as:

$$\Delta\varphi_{OFS,a} = \Delta\varphi_{MV}(f_1) - \Delta\varphi_{FIT}(f_1) \quad (16)$$

Also in this case, $\Delta\varphi_{MV}(f_1)$ is obtained from the tests carried out under the prescribed rated conditions (see section 3.2).

The phase error is assumed as $\Delta\varphi_{FIT}(f) + \Delta\varphi_{OFS,a}$ from the rated frequency up to f_{start} . From this frequency up to f_{stop} , the VT phase frequency response is equal to the low voltage phase error $\Delta\varphi_{LV}(f)$ shifted of the quantity $\Delta\varphi_{OFS,b}$ obtained as:

$$\Delta\varphi_{OFS,b} = \Delta\varphi_{FIT}(f_{start}) + \Delta\varphi_{OFS,a} - \Delta\varphi_{LV}(f_{start}) \quad (17)$$

Summarizing, the approximated phase error $\Delta\varphi_{S-LV}(f)$ is:

$$\Delta\varphi_{S-LV}(f) = \begin{cases} \Delta\varphi_{FIT}(f) + \Delta\varphi_{OFS,a} & f_1 \leq f < f_{start} \\ \Delta\varphi_{LV}(f) + \Delta\varphi_{OFS,b} & f_{start} \leq f < f_{stop} \end{cases} \quad (18)$$

The graphical representation of the S-LV steps is provided in Fig. 4, where all the involved curves are shown. The phase frequency response obtained under FH1 MV frequency sweep is also shown for comparison.

4. Measurement procedure and setup

4.1. Measurement procedure

As explained in section 3, S-LV requires two measurement steps that involve the generation of sinusoidal voltage waveforms only.

The first step, described also in section 3.2, consists in the determination of the VT ratio and phase errors at rated frequency f_1 , according to standard [17], performed by generating a sinusoidal voltage with amplitude from 80% to 120% of VT primary rated voltage.

The second step consists in a LV test, that is a sinusoidal frequency

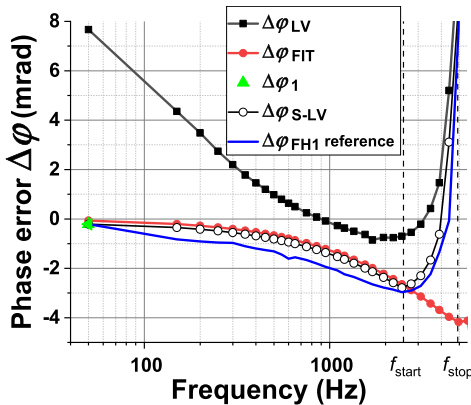


Fig. 4. Graphical representation of the S-LV steps for the identification of the VT phase error frequency response.

sweep from power frequency up to the first resonance frequency, performed at low voltage, e.g. 7 V. For each frequency f , the ratio and phase errors $\varepsilon_{LV}(f)$ and $\Delta\varphi_{LV}(f)$ are evaluated according to (2) and (3).

From these two measurement steps results, the VT frequency response in terms of ratio error $\varepsilon_{S-LV}(f)$ and phase error $\Delta\varphi_{S-LV}(f)$ is built, following the procedure explained in section 3.

4.2. Measurement setup

Two setups with different generation and measurement capabilities are used for step 1 and step 2.

As regards step 1, the VT characterization is carried out with the measurement setup shown in Fig. 5. The LV voltage signal is generated by the Arbitrary Waveform Generator (AWG) National Instrument (NI) PCI eXtension for Instrumentation (PXI) 5421, with 16 bit, variable output gain, ± 12 V output range, 100 MHz maximum sampling rate, 256 MB of onboard memory. The AWG is inserted in a PXI chassis and the 10 MHz PXI clock is used as a reference clock for its Phase Locked Loop (PLL) circuitry. The voltage waveform generated by the AWG is amplified by a Trek high-voltage power amplifier (± 30 kV, ± 20 mA) with wide bandwidth, high slew rate and low noise. The applied MV voltage values are scaled by a 30 kV wideband reference divider designed, built and characterized at INRIM [23]. The same generation system is also used for the validation of the S-LV procedure, that is for the execution of the FH1 tests, as better explained in section 5.

For step 2, the low voltage frequency sweep is performed by using a Fluke 5500A calibrator, remotely controlled, and no reference sensor is used, since the generated low voltage amplitude is always compliant with the input range of the acquisition system.

For both the measurement setups, the acquisition system is composed of a NI compact Data Acquisition system (cDAQ) chassis with various input modules, having 24 bit resolution, 50 kHz maximum sampling rate and input range from ± 500 mV up to ± 425 V. The magnitude and phasors of the primary and secondary voltages are extracted from the recorded voltage waveforms through an Interpolated Discrete Fourier Transform (IpDFT).

The overall uncertainty (level of confidence 95%) of the measurement setup in Fig. 5 ranges from 70 μ V/V and 70 μ rad at 50 Hz up to 200 μ V/V and 350 μ rad at 9 kHz for the ratio error and phase error, respectively.

As regards the setup for the low voltage frequency sweep, the sole uncertainty contribution source is due to the acquisition system. Following its calibration, its uncertainty is estimated equal to 50 μ V/V and 50 μ rad at power frequency and reaches 100 μ V/V and 120 μ rad at 9 kHz for the ratio error and phase error respectively.

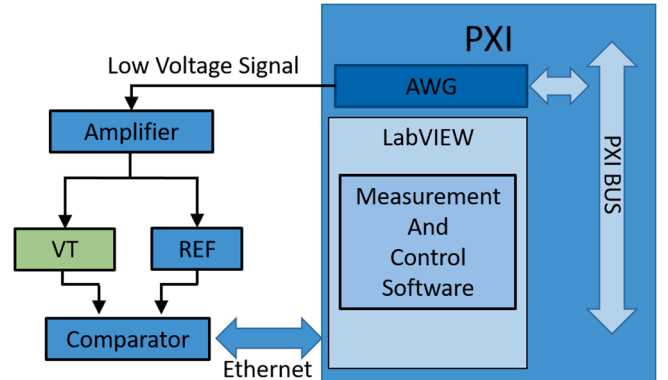


Fig. 5. Block diagram of the setup used for VT characterization in step 1 and for S-LV validation tests.

5. Validation of SINDICOMP-LV

The S-LV procedure is validated by applying it to the characterization of three commercial VTs (A, B and C) with different rated primary voltages and expected frequency behaviors. In details, Section 5.1 presents the VT specifications and the results of the fitting procedure. The application of S-LV to VT_A, VT_B and VT_C is then shown in sections 5.2, 5.3 and 5.4 respectively, where all the tests are carried out under null burden.

An estimation of the performance of the S-LV procedure in terms of its capability to better approximate the VT errors under distorted MV conditions is also carried out.

The performances of the proposed S-LV procedure are quantified as:

$$\begin{aligned}\delta_{S-LV}(f) &= \varepsilon_{S-LV}(f) - \varepsilon_{MV}(f) \\ \vartheta_{S-LV}(f) &= \Delta\varphi_{S-LV}(f) - \Delta\varphi_{MV}(f)\end{aligned}\quad (19)$$

where δ_{S-LV} , ϑ_{S-LV} are the deviations between the approximated ($\varepsilon_{S-LV}(f)$, $\Delta\varphi_{S-LV}(f)$) and actual ($\varepsilon_{MV}(f)$, $\Delta\varphi_{MV}(f)$) ratio and phase error respectively.

To quantify the improvement provided by the proposed procedure with respect to the simple low voltage single tone sweep, the deviations between the errors obtained at low voltage ($\varepsilon_{LV}(f)$, $\varphi_{LV}(f)$) and the actual ones are computed as:

$$\begin{aligned}\delta_{LV}(f) &= \varepsilon_{LV}(f) - \varepsilon_{MV}(f) \\ \vartheta_{LV}(f) &= \Delta\varphi_{LV}(f) - \Delta\varphi_{MV}(f)\end{aligned}\quad (20)$$

In both (19) and (20), the MV actual errors $\varepsilon_{MV}(f)$ and $\varphi_{MV}(f)$ are equal to those measured in the FH1 tests ($\varepsilon_{FH1}(f)$, $\varphi_{FH1}(f)$), which are assumed as reference errors. The FH1 tests are performed by using the INRIM reference system [23]. Fundamental tone with amplitude in the range 80% to 120% of the VT primary rated voltage and frequency 50 Hz, and one harmonic tone, with amplitude 1% of the fundamental one and frequency from 100 Hz up to 10 kHz, are used. For each generated harmonic tone, various phase angles in the range $\pm \pi$ rad are analyzed.

Measurements described in the following are carried out under controlled environmental conditions (temperature $23^\circ\text{C} \pm 1^\circ\text{C}$, relative humidity from 40% to 70%).

5.1. Devices under test and fit results

The VTs considered in this analysis are commercial resin insulated VTs for MV phase to ground measurement applications. The VTs main features are summarized in Table 1.

For each VT, the two steps required by S-LV are performed. As regards the LV test, the sinusoidal frequency sweep is executed at harmonic frequencies hf_1 from f_1 up to 10 kHz with a 7 V applied voltage.

Table 2 summarizes, for each analyzed VT, the selected fit frequency region and the fit parameters, obtained according to the procedure described in section 3.

5.2. VT_A characterization and S-LV validation

The deviations $\delta_{S-LV}(f)$ and $\delta_{LV}(f)$ versus frequency are shown in Fig. 6. The VT ratio errors measured by the FH1 reference test are given in the same figure (red triangular marker). Related numerical results for a limited number of frequencies are given in Table 3.

The VT_A ratio error ε_{FH1} is quite low (a few parts in 10^3) at the first

Table 2

Fit parameters of the analyzed VTs.

	f_R (Hz)	f_{start} (Hz)	f_{stop} (Hz)	a (s)	b
VT _A	5900	2450	4900	0.2	1.7
VT _B	9500	4000	8500	1	1
VT _C	2000	750	1000	0.65	1.5

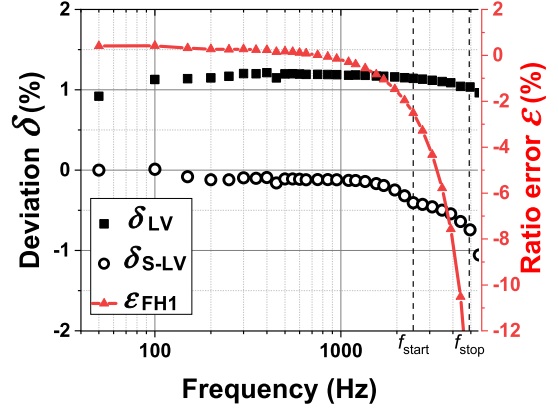


Fig. 6. Comparison between the VT_A ratio error deviations obtained by the LV (square marker) and the S-LV (circle marker) characterization. VT_A reference ratio error obtained performing the FH1 test (triangle marker) is also shown.

Table 3

VT_A ratio error results.

Frequency (Hz)	$\varepsilon_{FH1}(f)$ (%)	$\delta_{LV}(f)$ (%)	$\delta_{S-LV}(f)$ (%)
150	-0.092	1.14	-0.08
400	-0.17	1.22	-0.09
1200	-0.79	1.18	-0.15
3500	-6.16	1.10	-0.50
4900	-15.76	1.05	-0.75

harmonics and then increases up to -15.76% at 4.9 kHz (f_{stop}). If we analyze the LV deviation $\delta_{LV}(f)$ results, we can observe a reduction $\delta_{LV}(f)$ at highest frequencies, but worst results for the first harmonics, i. e. at the third harmonic, where $\delta_{LV}(f)$ is over one order of magnitude higher than the reference error. We can see, instead, that the S-LV approach gives better results for all the analyzed frequencies. In particular, for the first ten harmonics, the deviation values are lower than 0.1%, whereas an increase can be observed at the highest frequencies. Nevertheless, the highest absolute value is well below 1% and it is reached only at f_{stop} , i. e. 4.9 kHz.

The corresponding phase error deviations $\vartheta_{S-LV}(f)$ and $\vartheta_{LV}(f)$ and the VT reference phase error $\Delta\varphi_{FH1}(f)$ versus frequency are shown in Fig. 7, whereas related numerical results are given in Table 4.

Looking at Fig. 7, it can be noted that the deviations obtained with the LV characterization are the highest almost for every analyzed frequency, but especially for the first harmonics. On the contrary, the S-LV approach gives better results for each analyzed frequency and the absolute value of the phase error deviation remains lower than 1.1 mrad up to 4.9 kHz where the actual error is 8 mrad.

5.3. VT_B characterization and validation

The VT_B reference ratio errors $\varepsilon_{FH1}(f)$, and the deviations $\delta_{S-LV}(f)$ and $\delta_{LV}(f)$ versus frequency are shown in Fig. 8, whereas numerical results are given in Table 5.

Looking at the two ratio error deviation trends in Fig. 7, it can be noted that also for VT_B, the use of the S-LV procedure leads to the best results. For instance, at 2.1 kHz the deviation with respect to the FH1

Table 1

Rated characteristics of the analyzed VTs.

	Rated Primary Voltage (kV)	Rated Secondary Voltage (V)	Rated Burden (VA)	Accuracy class
VT _A	20/ $\sqrt{3}$	100/ $\sqrt{3}$	50	0.5
VT _B	11/ $\sqrt{3}$	110/ $\sqrt{3}$	50	0.5
VT _C	20	100	50	0.2

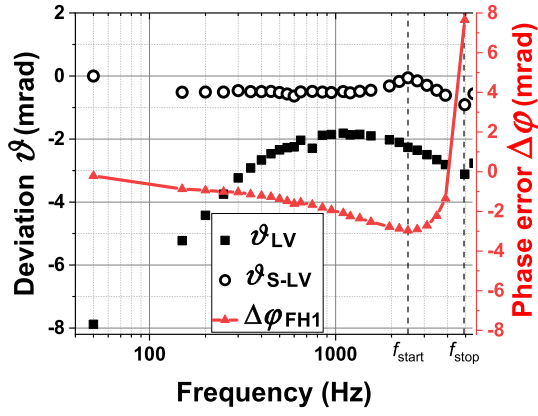


Fig. 7. Comparison between the VT_A phase error deviations obtained by the LV (square marker) and the S-LV (circle marker) characterization. VT_A reference phase error obtained performing the FH1 test (triangle marker) is also shown.

Table 4

VT_A phase error results.

Frequency (Hz)	$\Delta\varphi_{FH1}(f)$ (mrad)	$\vartheta_{LV}(f)$ (mrad)	$\vartheta_{S-LV}(f)$ (mrad)
150	-0.66	-5.23	-0.52
400	-0.99	-2.67	-0.50
1200	-2.03	-1.88	-0.54
3500	-2.02	-2.65	-0.58
4900	2.99	-3.10	-1.05

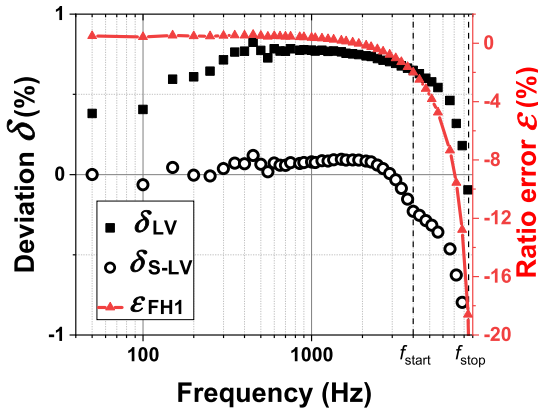


Fig. 8. Comparison between the VT_B ratio error deviations obtained by the LV (square marker) and the S-LV (circle marker) characterization. VT_B reference ratio error obtained performing the FH1 test (triangle marker) is also shown.

Table 5

VT_B ratio error results.

Frequency (Hz)	$\varepsilon_{FH1}(f)$ (%)	$\delta_{LV}(f)$ (%)	$\delta_{S-LV}(f)$ (%)
150	0.040	0.60	0.044
1500	-0.32	0.76	-0.094
2100	-0.65	0.66	-0.23
6100	-6.40	0.52	-0.42

value obtained by using the LV measurement is 0.66%, and it reduces to about one third (-0.23%) by using the proposed procedure.

The VT_B phase errors $\Delta\varphi_{FH1}(f)$ and the deviations $\vartheta_{S-LV}(f)$ and $\vartheta_{LV}(f)$ versus frequency are shown in Fig. 9, whereas the related numerical results are given in Table 6.

In this case, the application of S-LV to VT_B allows obtaining a phase error deviation (absolute value) lower than 1 mrad up to 7.2 kHz. In

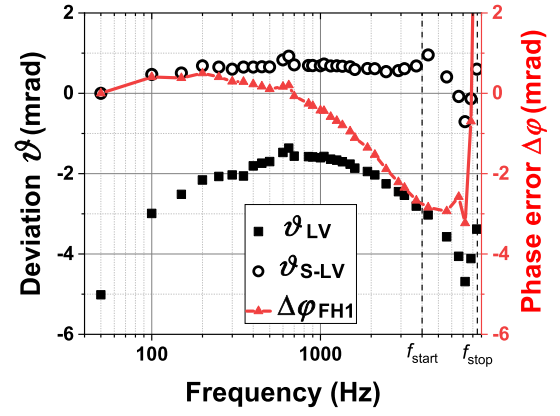


Fig. 9. Comparison between the VT_B phase error deviations obtained by the LV (square marker) and the S-LV (circle marker) characterization. VT_B reference phase error obtained performing the FH1 test (triangle marker) is also shown.

Table 6

VT_B phase error results.

Frequency (Hz)	$\Delta\varphi_{FH1}(f)$ (mrad)	$\vartheta_{LV}(f)$ (mrad)	$\vartheta_{S-LV}(f)$ (mrad)
150	0.38	-2.51	0.51
1500	-0.95	-1.76	0.66
2100	-1.53	-2.05	0.60
6100	-2.80	-3.80	0.19

particular, for VT_B , the improvement obtained for the phase error, as the frequency increases, is more evident than the one obtained with VT_A .

5.4. VT_C characterization and validation

The VT_C ratio errors $\varepsilon_{FH1}(f)$ and the deviations $\delta_{S-LV}(f)$ and $\delta_{LV}(f)$ are shown in Fig. 10. Some numerical results are also given in Table 7.

The application of the S-LV method to VT_C leads to a significant reduction of the ratio error deviation, whose maximum value is -0.36%.

The corresponding phase error deviations and the reference response versus frequency are shown in Fig. 11; related numerical results are given in Table 8.

As regards the phase error deviation, $\vartheta_{S-LV}(f)$ is within 0.5 mrad up to 1 kHz, whereas, in the same frequency range, $\vartheta_{LV}(f)$ reaches a maximum value of -5.20 mrad.

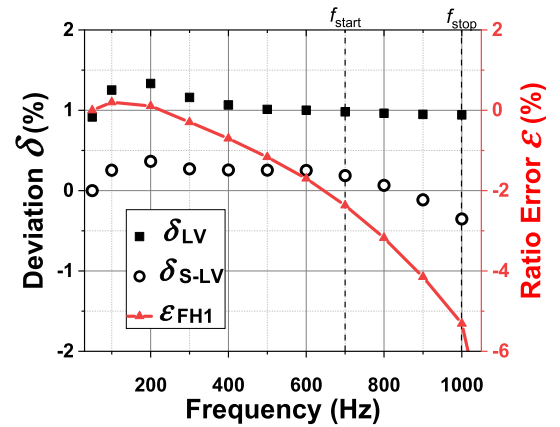


Fig. 10. Comparison between the VT_C ratio error deviations obtained by the LV (square marker) and the S-LV (circle marker) characterization. VT_C reference ratio error obtained performing the FH1 test (triangle marker) is also shown.

Table 7VT_C ratio error results.

Frequency (Hz)	$\varepsilon_{FH1}(f)$ (%)	$\delta_{LV}(f)$ (%)	$\delta_{S-LV}(f)$ (%)
200	0.11	1.33	0.36
400	0.70	1.07	0.26
800	-3.18	0.97	0.066
1000	-5.31	0.95	-0.35

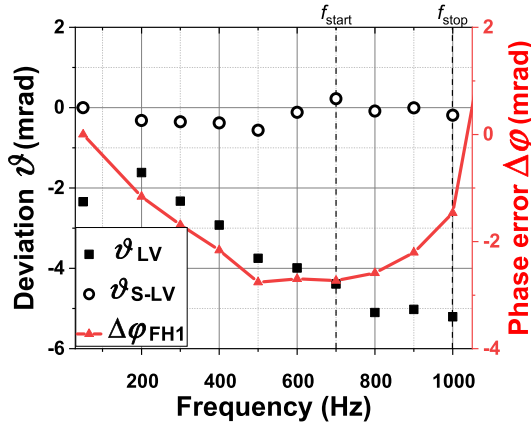


Fig. 11. Comparison between the VT_C phase error deviations obtained by the LV (square marker) and the S-LV (circle marker) characterization. VT_C reference phase error obtained performing the FH1 test (triangle marker) is also shown.

Table 8VT_C phase error results.

Frequency (Hz)	$\Delta\varphi_{FH1}(f)$ (mrad)	$\vartheta_{LV}(f)$ (mrad)	$\vartheta_{S-LV}(f)$ (mrad)
200	-1.16	-1.61	-0.32
400	-2.16	-2.92	-0.38
800	-2.10	-5.10	-0.084
1000	-0.87	-5.20	-0.19

6. Sensitivity analysis of S-LV

The accuracy performances of the S-LV procedure, as investigated in the previous section, can be affected by the value assumed for the influence quantities. Three quantities are considered in the following: two of them are parameters of the method, f_{start} and the amplitude of the sinusoidal voltage used in the LV test, and the third is the burden used in the VT operation.

For sake of brevity, the analyses here shown refer only to the ratio error of VT_A. Similar considerations can be done for the other two VTs and are also valid for phase error.

6.1. S-LV sensitivity to f_{start} selection

The scope of this section is to quantify the impact of the f_{start} choice on the S-LV accuracy performance. For this purpose, the factor m , indicated in (10) as the value that allows obtaining the best results, is varied in the range [2,3] with a step equal to 0.25. Thus, five different f_{start} values are used in the S-LV technique application, given in Table 9.

The assessment of the f_{start} impact on the S-LV performance is shown

Table 9Values of f_{start} chosen to verify S-LV sensitivity.

m	2	2.25	2.5	2.75	3
f_{start} (Hz)	3000	2750	2450	2200	1950

in Fig. 12. The triangle represents the reference ratio error $\varepsilon_{FH1}(f)$, whereas the circle represents, for each frequency, the value of the $\delta_{S-LV}(f)$ obtained with the five different f_{start} values. The bars superimposed to the circles are the maximum deviation from the mean value. It can be observed that the bars are practically null up to 2 kHz, where they start to be detectable.

The maximum bar amplitude, found at f_{stop} , is below 0.2% against a deviation value of 0.75%. This proves the substantial insensitivity of S-LV to f_{start} at low frequencies and the quite limited effect when approaching the resonance frequency.

6.2. S-LV sensitivity to LV amplitude selection

The analysis carried out in the previous sections refers to LV tests carried out at the lower considered value (7 V). Six low voltage amplitudes are here considered: 7 V, 10 V, 20 V, 50 V, 100 V and 200 V and the S-LV procedure is executed for each considered voltage amplitude.

As regards the identification of f_R , no difference is found and, consequently, the values of f_{start} and f_{stop} are the same for each considered low voltage level. As to the fit parameters, they slightly decrease with the increase of the low voltage amplitude. In particular, b and a found at 7 V are 1.7 and 0.2 s, whereas they drop to 1.58 and 0.19 s at 200 V. The resulting S-LV ratio error deviation curves are shown in Fig. 13, along with $\varepsilon_{FH1}(f)$. Fig. 14 shows a zoom of Fig. 13, depicting only the $\delta_{S-LV}(f)$ curves.

All the S-LV deviations curves are well overlapped from 50 Hz up to 2450 Hz and no significant differences are measured. From 2450 Hz up to 4900 Hz the difference among the curves can be appreciated: in particular, at 4900 Hz the reduction of $\delta_{S-LV}(f)$ can be clearly observed. However, the maximum deviation between 7 V and 200 V, at 4900 Hz, is equal to 0.12% that represents a relative benefit, compared to the eventual rising cost if the instrumentation necessary to increase the test voltage over 7 V has to be purchased.

6.3. S-LV sensitivity to VT burden condition

The aim of this section is to assess the impact of the VT burden condition on the S-LV performance. For this purpose, VT_A has been characterized under its rated burden condition [17], i.e. using a 50 VA ohmic-inductive burden with a $\cos\varphi_b = 0.8$ active factor.

As a preliminary verification, the deviation between the ratio error $\varepsilon_{S-LV}(f)$ found with zero burden condition and the reference response $\varepsilon_{FH1,rb}(f)$ measured when the VT_A supplies its rated burden is evaluated. Results related to this analysis are shown in Fig. 15. Looking at Fig. 15, it is evident that the results are unsatisfactory. In fact, for the first

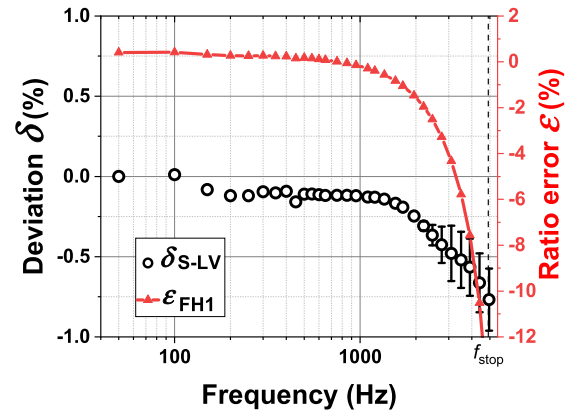


Fig. 12. Sensitivity analysis of S-LV to f_{start} . Reference ratio error of VT_A $\varepsilon_{FH1}(f)$ (triangle marker) and mean values of $\delta_{S-LV}(f)$ (circle marker) of the f_{start} values. The bars over the circle marker represent the maximum deviations from the mean values.

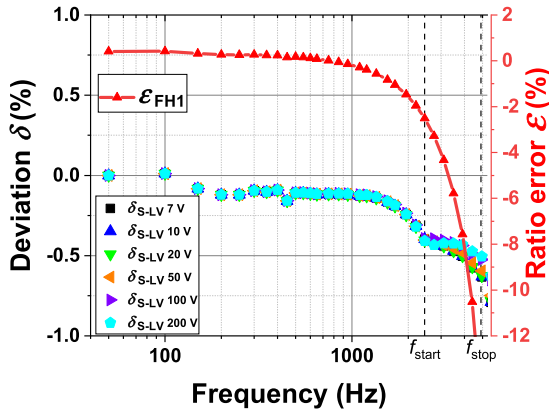


Fig. 13. Comparison between the $\mathcal{E}_{FH1}(f)$ ratio error of VT_A (triangle marker) and the ratio error deviations $\delta_{S-LV}(f)$ (various triangle markers) obtained with different LV amplitudes.

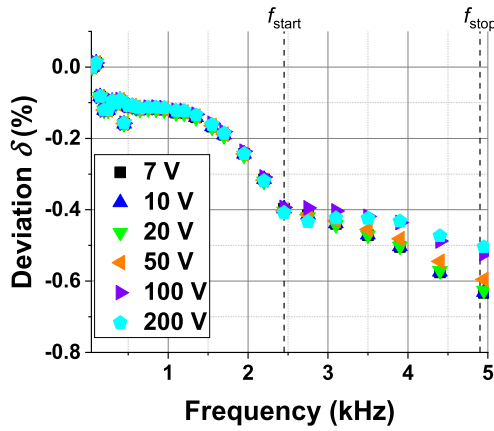


Fig. 14. Ratio errors deviations $\delta_{S-LV}(f)$ obtained with increasing LV voltage amplitude (zoomed data).

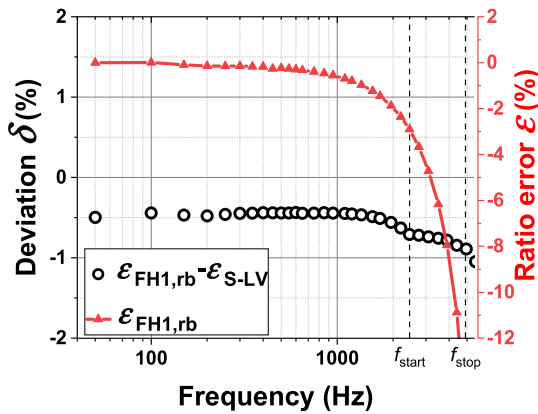


Fig. 15. Ratio error of VT_A with rated burden $\mathcal{E}_{FH1,rb}(f)$, obtained by performing the FH1 test (triangle marker), and the deviation between $\mathcal{E}_{S-LV}(f)$ and $\mathcal{E}_{FH1,rb}(f)$ (circle marker).

harmonics the S-LV deviation error is equal to 0.5%, that is about seven times higher than the results obtained with zero burden condition. This result is mainly due to an evident performance variation of the VT in presence of the burden. In this regard, it is sufficient to point out that burden strongly varies the ratio error at power frequency from 0.41% (zero burden) to -0.09% (rated burden).

In light of this, as expected, it is necessary to carry out the S-LV

procedure for each rated burden condition, under which the VT is designed to operate.

As regards the fit frequency region identification, it should be taken into account that the burden does not change the first frequency resonance point [22], so it is not necessary to repeat the identification of f_R , f_{start} and f_{stop} , since the values are the same as those found with zero burden.

As to the fit parameters, b and a have higher values in presence of the burden: b increases from 1.7 to 2.40 whereas a goes from 0.2 s to 0.21 s.

Results related to this analysis are shown in Fig. 16 where the reference ratio errors $\mathcal{E}_{FH1,rb}(f)$, $\delta_{S-LV,rb}(f)$ and $\delta_{LV,rb}(f)$ are shown.

Similarly, to the zero burden case, the S-LV method strongly reduces the ratio error deviations, by giving values below 0.1% up to 1500 Hz, whereas the maximum error is found at 4950 Hz and equal to -0.6% .

7. Discussion of results

From the analysis of the results shown in section 5 and 6 for the three different MV VTs, some general considerations can be made with reference to the accuracy associated with the frequency response results obtained by application of the S-LV procedure.

If we focus the attention on the ratio error up to 1 kHz it can be observed that for both VT_A and VT_B (Fig. 6 and Fig. 10), the application of the S-LV technique allows the determination of the VT frequency response with residual deviations $\delta_{S-LV}(f)$ down to less than 0.1% (absolute value). These residual deviations have to be compared with the about one order of magnitude higher deviations $\delta_{LV} = 1.12\% \pm 0.1\%$ (VT_A) and 0.77% (VT_B), found when the LV voltage approach is used. For the highest frequencies, where the linear capacitive effect becomes predominant, the deviations $\delta_{S-LV}(f)$ increase, up to 0.75% and 0.42% at f_{stop} , being always more than ten times lower than the actual errors to be measured. As regards VT_C , the $\delta_{S-LV}(f)$ residual deviations at low frequencies are higher with respect to the other examined VTs, being of the order of a few part in 10^3 . This behavior can be explained considering that the VT_C resonance frequency is quite low, so that, even at the lower harmonics, the linear stray capacitive effects are present and superimposed to the core non-linear effects, so decreasing the effectiveness of the SINDICOMP procedure.

As to the phase errors deviations $\vartheta_{S-LV}(f)$, they range from less than 0.2 mrad to 0.8 mrad (absolute values), up to frequencies close to f_R . These values have to be compared with the $\vartheta_{LV}(f)$ ones, which varies from 2 mrad to 5 mrad (absolute values), so with a not negligible increase in the accuracy of the residual error estimate.

These considerations are valid also when $\delta_{S-LV}(f)$ is measured at 200 V. In fact, a detectable reduction of the residual error due to the increased value of the applied LV signal is found only starting from some kilohertz for VT_A , but the improvement in the reproduction of the VT

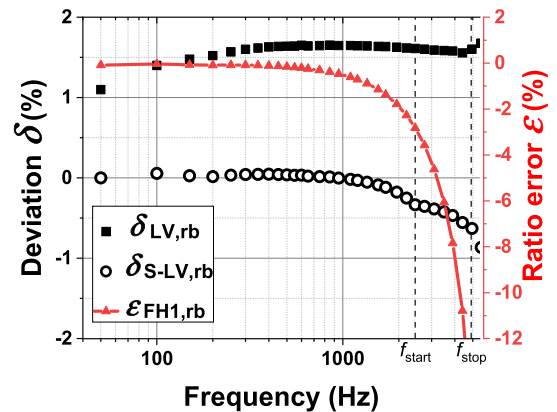


Fig. 16. Ratio error deviation of VT_A with rated burden, obtained by the LV (square marker) and S-LV (circle marker) procedure.

frequency response is not so significant at least up to a frequency close to the resonance one.

A quite limited effect is linked to the choice of the frequency range. To this end, the effects of the sensitivity analysis on f_{start} , as described in Section 6.1, is considered. In this case a visible effect is present starting from a few kilohertz, but again the variation in the residual error due the f_{start} is of a few parts in 10^3 , but at frequencies higher than 3 kHz.

The sensitivity analysis related to the burden condition shown in Section 6.3 highlights the importance of characterizing the VTs at each operating burden. For example, Fig. 15 shows that not considering the burden effect leads to an increase of ratio error deviation from 0.5% at rated frequency to 1% at 5 kHz.

8. Conclusion

This paper has presented an industry oriented technique for the accurate frequency characterization of MV inductive VTs up to close the first resonance frequency. The SINDICOMP-LV involves the generation of only sinusoidal voltage waves with instrumentation that, typically, is already present in accredited VT calibration laboratories or at VT manufacturer premises. S-LV technique consists of two steps, where the first one involves the application of the same MV voltages and test burden at rated frequency as those applied in VT calibration tests carried out according to the relevant technical standard. The second step is a sinusoidal frequency sweep carried out at very LV, down to 7 V.

The technique has been validated and its accuracy limits estimated by the INRIM reference system for VT frequency characterization, under MV voltages representative of distorted grid conditions. Results of validation tests performed applying the S-LV procedure to MV VTs with rated primary voltages from $11/\sqrt{3}$ kV to 20 kV demonstrated that:

- the S-LV procedure allows the estimation of the ratio and phase errors of the VT, with respect to those measured under distorted MV voltage by using the INRIM reference measurement systems;
- sensitivity analysis shows that it is quite robust to a different choice for its parameters;
- for all the three investigated VTs, the estimate of the S-LV accuracy performance in the VT ratio error evaluation is found within $4 \cdot 10^{-3}$ up to 20th harmonic, and within 1% close to the resonance frequency; as to the phase error, it is always within 0.8 mrad;
- accuracy improvement with respect to the use of a conventional low voltage frequency sweep technique is up to one order of magnitude for the ratio error and up to 5 mrad for the phase over the considered frequency ranges, depending on the frequency value;
- a further significant advantage of the S-LV technique is that, with respect to the costlier set-ups which do allow to carry out the frequency analysis under conditions closer to the on-site ones, it can be simply implemented by using the generation and measurement setups already available in VT calibration laboratories.

CRediT authorship contribution statement

G. Crotti: Methodology, Validation, Investigation, Writing - original draft, Writing - review & editing, Supervision, Project administration, Funding acquisition. **D. Giordano:** Conceptualization, Validation, Formal analysis, Writing - original draft, Writing - review & editing. **G. D'Avanzo:** Software, Writing - original draft, Writing - review & editing. **P.S. Letizia:** Methodology, Software, Validation, Formal analysis, Investigation, Writing - original draft, Writing - review & editing, Visualization. **M. Luiso:** Conceptualization, Writing - original draft, Writing - review & editing, Supervision, Funding acquisition.

Declaration of competing interest

The authors declare that they have no known competing financial interests or personal relationships that could have appeared to influence

the work reported in this paper.

Acknowledgments

The work presented in this paper was developed within the 19NRM05 IT4PQ project which has received funding from the EMPIR programme cofinanced by the participating States and from the European Union's Horizon 2020 research and innovation programme.

Appendix A. Supplementary material

Supplementary data to this article can be found online at <https://doi.org/10.1016/j.measurement.2021.109674>.

References

- [1] S. Bhattacharyya and S. Cobben: "Consequences of Poor Power Quality – An Overview", 2011, DOI: 10.5772/13787.
- [2] S. Elphick, V. Gosbell, V. Smith, S. Perera, P. Ciuffo, G. Drury, *Methods for Harmonic Analysis and Reporting in Future Grid Applications*, IEEE Trans. Power Del. 32 (2) (2017) 989–995.
- [3] L. Peretto, *The role of measurements in the smart grid era*, IEEE Instrum. Meas. Mag. 13 (3) (2010) 22–25.
- [4] D. Vieira, R.A. Shayani, M.A.G. de Oliveira, *Reactive Power Billing under Nonsinusoidal Conditions for Low-Voltage Systems*, IEEE Trans. Instrum. Meas. 66 (8) (2017) 2004–2011.
- [5] G. D'Avanzo, A. Delle Femine, D. Gallo, C. Landi, M. Luiso, "Impact of inductive current transformers on synchrophasor measurement in presence of modulations", *Measurement*, Volume 155, 2020, 107535.
- [6] T. Pfajfar, J. Meyer, P. Schegner, e I. Papić, "Influence of instrument transformers on harmonic distortion assessment", in 2012 IEEE Power and Energy Society General Meeting, Aug. 2012, page. 1–6, doi: 10.1109/PESGM.2012.6345309.
- [7] A. Cataliotti, D. Di Cara, A.E. Emanuel, S. Nuccio, *A Novel Approach to Current Transformer Characterization in the Presence of Harmonic Distortion*, IEEE Trans. Instrum. Meas. 58 (5) (May 2009) 1446–1453.
- [8] M. Faifer, et al., *Overcoming Frequency Response Measurements of Voltage Transformers: An Approach Based on Quasi-Sinusoidal Volterra Models*, IEEE Trans. Instrum. Meas. 68 (8) (Aug. 2019) 2800–2807.
- [9] A. Cataliotti, et al., *Compensation of Nonlinearity of Voltage and Current Instrument Transformers*, IEEE Trans. Instrum. Meas. 68 (5) (May 2019) 1322–1332.
- [10] S. Toscani, M. Faifer, A. Ferrero, C. Laurano, R. Ottoboni, M. Zanoni, *Compensating Nonlinearities in Voltage Transformers for Enhanced Harmonic Measurements: The Simplified Volterra Approach*, IEEE Trans. Power Del. 36 (1) (2021) 362–370, <https://doi.org/10.1109/TPWRD.2020.2978668>.
- [11] M. Klatt, J. Meyer, M. Elst, and P. Schegner, "Frequency Responses of MV voltage transformers in the range of 50 Hz to 10 kHz", in Proceedings of 14th International Conference on Harmonics and Quality of Power - ICHQP 2010, Sept. 2010, pp. 1–6, doi: 10.1109/ICHQP.2010.5625484.
- [12] A.J. Collin, A. Delle Femine, D. Gallo, R. Langella, M. Luiso, *Compensation of Current Transformers' Nonlinearities by Tensor Linearization*, IEEE Trans. Instrum. Meas., Oct. 68 (10) (2019) 3841–3849.
- [13] R. Stiegler, J. Meyer, and P. Schegner, "Portable measurement system for the frequency response of voltage transformers", in 2012 IEEE 15th International Conference on Harmonics and Quality of Power, June. 2012, pp. 745–750, doi: 10.1109/ICHQP.2012.6381233.
- [14] G. Crotti, D. Gallo, D. Giordano, C. Landi, M. Luiso, and M. Modarres, "Calibration of MV voltage instrument transformer in a wide frequency range", in 2017 IEEE International Instrumentation and Measurement Technology Conference (I2MTC), May. 2017, pp. 1–6, doi: 10.1109/I2MTC.2017.7969770.
- [15] IEC 61869-1:2007, *Instrument transformers - Part 1: General requirements*.
- [16] IEC 61869-2:2012, *Instrument transformers - Part 2: Additional requirements for current transformers*.
- [17] IEC 61869-3:2011, *Instrument transformers - Part 3: Additional requirements for inductive voltage transformers*.
- [18] EMPIR 19NRM05 IT4PQ project website, available online on 08 June 2021 at https://www.euramet.org/research-innovation/search-research-projects/details/project/measurement-methods-and-test-procedures-for-assessing-accuracy-of-instrument-transformers-for-power/?L=0&tx_eurametctcp_project%5Baction%5D=show&tx_eurametctcp_project%5Bcontroller%5D=Project&cHash=022ee6ab2e8ea8c12a7ed904625a1cc7.
- [19] G. Crotti et al., "Measurement Methods and Procedures for Assessing Accuracy of Instrument Transformers for Power Quality Measurements," 2020 Conference on Precision Electromagnetic Measurements (CPEM), Denver (Aurora), CO, USA, 2020, pp. 1–2.
- [20] P. S. Letizia et al., "Low Cost Procedure for Frequency Characterization of Voltage Instrument Transformers," 2019 IEEE International Instrumentation and Measurement Technology Conference (I2MTC), Auckland, New Zealand, 2019, pp. 1–6.
- [21] G. Crotti, D. Giordano, P.S. Letizia, A. Delle Femine, M. Luiso, "A simplified procedure for the accurate frequency response identification of voltage

- transformers", 24th IMEKO TC4 International Symposium and 22nd International Workshop on ADC and DAC Modelling and Testing, Palermo, Italy 14–16 (September 2020) 50–54.
- [22] C. Buchhagen, M. Fischer, L. Hofmann, and H. Däumling, «Metrological determination of the frequency response of inductive voltage transformers up to 20 kHz», in 2013 IEEE Power Energy Society General Meeting, July 2013, pp. 1–5.
- [23] G. Crotti et al., "Frequency Compliance of MV Voltage Sensors for Smart Grid Application," in IEEE Sensors Journal, vol. 17, no. 23, pp. 7621-7629, 1 Dec.1, 2017.